

Coupler enabled tunable dipole-dipole coupling between optically levitated nanoparticles

MIAN WU,¹ NAN LI,^{1,*} HAN CAI,^{1,*} AND HUIZHU HU^{1,*}

¹State Key Laboratory of Modern Optical Instrumentation, College of Optical Science and Engineering, Zhejiang University, Hangzhou 310027, China

*nanli@zju.edu.cn

*hancai@zju.edu.cn

*huhuizhu2000@zju.edu.cn

Abstract: Multiple optically levitated particles in vacuum can exhibit electrostatic interactions, optical binding, or non-reciprocal light-induced dipole-dipole interactions, making them promising platforms for exploring mesoscopic entanglement and complex interactions. However, in optical trap arrays, individually controlling the position and polarization of each trap is challenging, limiting the precise tuning of interactions between adjacent particles. This constraint hinders the study of complex interaction systems. In this work, we introduce a third nanoparticle as a coupler to two initially non-interacting nanoparticles, achieving tunable dipole-dipole coupling mediated by the third one. We investigated the effect of the particles' phases and positions on the interaction strength and demonstrated its broad tunability. Our method allows for precise control of interactions between any pair of adjacent particles in multi-particle systems, facilitating the further use of levitated nanoparticle arrays in entanglement research and sensing.

1. Introduction

Optically levitated nanoparticles [1–3] have emerged as a promising platform for precision sensing [4–9], the study of active matter [10–12], and the exploration of macroscopic quantum states [13–16]. Due to their excellent isolation from the environment, optically levitated nanoparticles can be cooled to the quantum ground state of their center-of-mass motion [17–24], paving the way for investigating quantum decoherence mechanisms and exploring the boundary between quantum and classical regimes.

Similar to optical tweezer arrays of levitated microscopic atoms or molecules, arrays of levitated macroscopic nanoparticles [25] with tunable dipole-dipole coupling are recognized as essential for achieving macroscopic entanglement [14, 16] and exotic topological quantum states [26, 27]. Interestingly, the coupling between optically levitated nanoparticles can be Hermitian or non-Hermitian due to scattering interactions, introducing a wide range of phenomena, including limit cycles [28, 29] and other exotic behaviors [30–35].

However, the coupling between nanoparticles depends on the intensity and polarization of the trapping laser [36]. Adjusting the trapping laser at any site inevitably alters the coupling coefficients with all neighboring particles. Although cavity-mediated interactions [35] can couple two nanoparticles over long distances, significant challenges remain in achieving independently controlled coupling coefficients between pairs of particles, hindering the tunable lattice engineering. Fortunately, this difficulty has been addressed in other quantum systems, particularly in superconducting qubit arrays. It has been found that introducing an additional qubit as a coupler between any two qubits allows for the individual tuning of coupling coefficients between pairs of qubits [37].

Here we demonstrate that an ancillary silica nanoparticle can mediate the coupling between the dipole-dipole interactions between other two nanoparticles, without requiring any inherent interaction between the two particles, as shown in Fig. 1(a). We investigate how the dipole-dipole interactions mediated by the third particle vary with the phase difference, interparticle distances, and relative positions between the three particles, demonstrating the tunability of the interaction

strength. Our work provides a novel approach for precisely controlling interactions between adjacent particles in multi-body systems, bypassing the problem of untunable position and polarization of each optical trap in optical trap arrays. This will facilitate the construction of larger-scale, fully programmable mechanical oscillator arrays and further applications in macroscopic quantum mechanics [13–15] and stochastic thermodynamics [38].

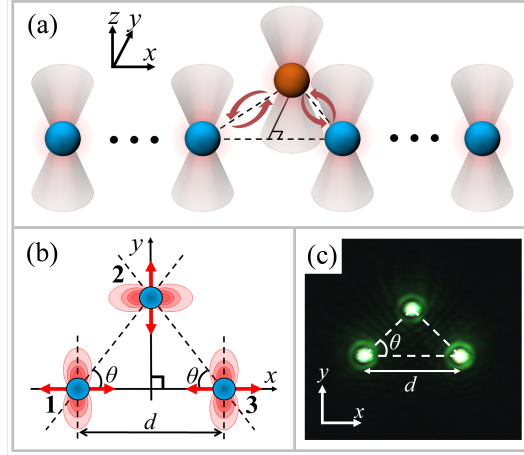


Fig. 1. (a) Schematic of light-induced dipole-dipole interactions between two optically levitated nanoparticles mediated by a third one. The blue particles represent a one-dimensional optical trap array composed of multiple particles, while the orange particle represents a particle acting as a coupler to mediate interactions between any pair of adjacent particles in the optical trap array. The red arrows represent light-induced dipole-dipole interactions between the particles. (b) In the focal plane, particle 1, particle 2, and particle 3 are trapped in trap 1, trap 2, and trap 3, respectively. Trap 1 and trap 3 are distributed along the x axis, with their polarization aligned along the x axis. Trap 2 is located on the perpendicular bisector of the line segment connecting trap 1 and trap 3, and its polarization is parallel to the y axis. The angle between the line connecting trap 1 and trap 2 and the x axis is θ , and the same applies to the line connecting trap 2 and trap 3. The spacing between trap 1 and trap 3 is d . The figure also illustrates the characteristic spatial profiles of the dipole radiation in the far field. (c) Camera image of three nanoparticles trapped in three optical traps under 532 nm laser illumination ($\theta \approx 45^\circ$, $d \approx 4.24 \mu\text{m}$).

2. Theoretical model

In our experiment, the wavelength of the trapping laser ($\lambda = 1064 \text{ nm}$) significantly exceeds the radius of silica nanoparticles ($r_p \approx 100 \text{ nm}$). In this case, the nanoparticles can be regarded as induced dipoles driven by the light field. The total light field of a particle is the sum of the trapping field and the scattered light from other particles, and the interference between these two fields causes the interactions between the particles. If there is phase difference between the trapping fields at the positions of the particles, the interactions between particles will be non-reciprocal because the scattered field obtains an extra phase when propagating between particles [36].

As shown in Fig. 1(b), we set up three optical traps in the focal plane ($x-y$ plane) perpendicular to the optical axis (z axis). Trap 1 and trap 3 are distributed along the x axis and symmetrical relative to the y axis, with linear polarization parallel to the x axis. In this configuration, the dipole-dipole interactions between particle 1 and particle 3 in trap 1 and trap 3 can be eliminated

due to the characteristic spatial profile of the dipole radiation in the far field. An additional trap 2, with a polarization along the y axis and orthogonal to the polarization of trap 1 and trap 3, is set up on the perpendicular bisector of the line segment connecting trap 1 and trap 3. Therefore, the particle 2 in trap 2 can act as a coupler to mediate the interactions between particle 1 and particle 3. We define the angle between the line connecting trap 1 and trap 2 and the x axis as θ , and the same applies to the line connecting trap 2 and trap 3. And the interparticle distance between trap 1 and trap 3 is d . Therefore, the distance between trap 1 and trap 2 is $d' = d/(2 \cos \theta)$, and the distance between trap 2 and trap 3 is the same. The intrinsic mechanical frequencies of the particle 1 and particle 3 are given by $\Omega_1 = \Omega_3 = \sqrt{1 + \eta} \cdot \Omega$, and the intrinsic mechanical frequency of particle 2 is $\Omega_2 = \sqrt{1 - 2\eta} \cdot \Omega$. Where η represents the power difference ($\Omega_i \propto \sqrt{P_i}$, here, P_i represents the trapping power of particle i), and Ω is the intrinsic mechanical frequency when $\eta = 0$ with no dipole-dipole interactions. In addition, the phase difference between trap 1 and trap 3 is π , and the phase difference between light trap 1 and trap 2 is $\Delta\varphi$, so the phase difference between light trap 2 and trap 3 is $\pi - \Delta\varphi$.

Previous experiments have shown that the coupling rate along the z direction is significantly greater than along the other directions [36], so we mainly explore interactions along the z direction. The detailed derivation of the dipole-dipole interactions between two particles in two orthogonally polarized traps is presented in Section 1 of Supplement 1. Here we assume the non-reciprocal coupling coefficient between particle 1 and particle 2 as $k_1 \pm k_2$, where k_1 represents the conservative part of the interactions and k_2 represents the non-conservative part of the interactions. In this case, the coupling coefficient from particle 2 to particle 1 is $k_1 + k_2$, and from particle 1 to particle 2 is $k_1 - k_2$. Here, k_1 and k_2 is given by the following expression:

$$k_1 = G \sin(2\theta) \cos\left(\frac{kd}{2 \cos \theta}\right) \cos(\Delta\varphi) / \left(\frac{kd}{2 \cos \theta}\right) \quad (1)$$

$$k_2 = G \sin(2\theta) \sin\left(\frac{kd}{2 \cos \theta}\right) \sin(\Delta\varphi) / \left(\frac{kd}{2 \cos \theta}\right) \quad (2)$$

Here, G is a constant that is positively related to the trapping power and the particle polarizability. Considering the phase difference $\pi - \Delta\varphi$ between particle 2 and particle 3, the coupling constant from particle 3 to particle 2 is $-k_1 + k_2$, and from particle 2 to particle 3 is $-k_1 - k_2$. We can now derive the linear dynamics equations for the system composed of the three optically levitated particles:

$$\begin{cases} m\ddot{z}_1 + m\gamma\dot{z}_1 + m(1 + \eta)\Omega^2 z_1 + (k_1 + k_2)(z_1 - z_2) = 0 \\ m\ddot{z}_2 + m\gamma\dot{z}_2 + m(1 - 2\eta)\Omega^2 z_2 + (k_1 - k_2)(z_2 - z_1) + (-k_1 + k_2)(z_2 - z_3) = 0 \\ m\ddot{z}_3 + m\gamma\dot{z}_3 + m(1 + \eta)\Omega^2 z_3 + (-k_1 - k_2)(z_3 - z_2) = 0 \end{cases} \quad (3)$$

Here, z_i represents the coordinate of the particle i along the optical axis, and the three particles share the same mass m . Furthermore, we assume $\Delta\varphi = 0$, thereby setting $k_2 = 0$ and turning the non-reciprocal interactions off. Then we can obtain three eigenfrequencies $\omega_{1,2,3}$ and the corresponding eigenvectors of the coupled harmonic oscillators by solving Eqs. (3). It is worth mentioning that in our previous experiment, we measured the coupling coefficient in the presence of particle 1 and particle 2. When the common intrinsic mechanical frequency of two particles was $\Omega \approx 47 \cdot 2\pi$ kHz, the angle was $\theta = 45^\circ$, the phase difference was $\Delta\phi = 0$, and the distance was $d = 3.11 \mu\text{m}$, we measured the value of the conservative coupling coefficient $k_1/m\Omega \approx 6.0 \cdot 2\pi$ kHz. From this value, we can further estimate the conservative coupling coefficient in other cases, which will be used for subsequent simulations.

Since the equations do not have analytical solutions, to illustrate how the dipole-dipole interactions vary with the distance d , we solve for the eigenfrequencies $\omega_{1,2,3}$ using parameters

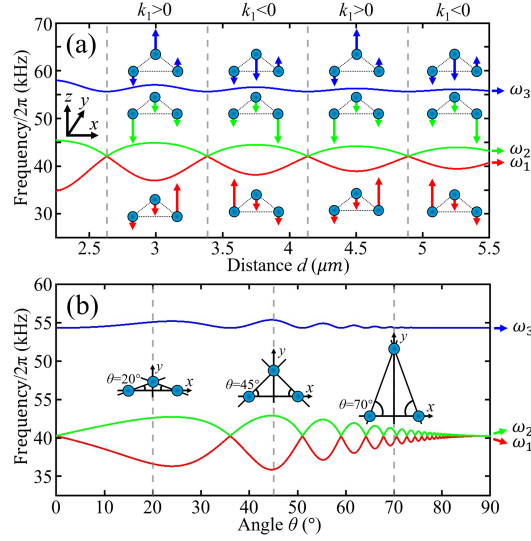


Fig. 2. (a) The eigenfrequencies $\omega_{1,2,3}$ of the coupled oscillators vary with the interparticle distance d at $\theta = 45^\circ$, $\Omega \approx 47 \cdot 2\pi$ kHz, $\eta \approx -0.2$, and $\Delta\varphi = 0$. The curve exhibits a periodicity of $\sqrt{2}\lambda/2$. Additionally, the motion states of particle 1, particle 2, and particle 3 along the z axis in the three normal modes of the system are illustrated in the figure. (b) The eigenfrequencies $\omega_{1,2,3}$ of the coupled oscillators vary with the angle θ at $d = 3.01 \mu\text{m}$, $\Omega \approx 47 \cdot 2\pi$ kHz, $\eta \approx -0.2$, and $\Delta\varphi = 0$. This figure also shows the distribution diagrams of three optical traps in the x - y plane at angles $\theta = 20^\circ$, $\theta = 45^\circ$, and $\theta = 70^\circ$.

close to the experimental conditions ($\theta = 45^\circ$, $\Omega \approx 47 \cdot 2\pi$ kHz, $\eta \approx -0.2$, $k_1/m\Omega \approx 6.0 \cdot 2\pi$ kHz @ $d = 3.11 \mu\text{m}$). As shown in Fig. 2(a), the eigenfrequencies $\omega_{1,2,3}$ of the coupled harmonic oscillators vary with a period of $\sqrt{2}\lambda/2$ as the distance d increases. In the two normal modes ω_1 and ω_2 , the oscillation amplitudes of particle 1 and particle 3 are large, indicating that ω_1 and ω_2 are their main oscillation modes. In addition, particle 1 and particle 3 oscillate inversely in the normal mode ω_1 , while particle 1 and particle 3 oscillate in the same phase in the normal mode ω_2 , similar to the breathing mode and center-of-mass mode in two-oscillator systems. The difference between ω_1 and ω_2 almost perfectly matches the variation of $|k_1|$ with distance d . Therefore, we define the normal mode splitting as $|\omega_2 - \omega_1|$ and use it to characterize the conservative interaction strength between particle 1 and particle 3 in subsequent experiments, and observe its variation with the distance d , the angle θ , and the phase difference $\Delta\varphi$.

Additionally, we simulated the variation of the eigenfrequencies $\omega_{1,2,3}$ with the angle θ (other parameters: $d = 3.01 \mu\text{m}$, $\Omega \approx 47 \cdot 2\pi$ kHz, $\eta \approx -0.2$). As shown in Fig. 2(b), the eigenfrequencies vary with θ , and the normal mode splitting $|\omega_2 - \omega_1|$ reaches its maximum when $\theta \approx 45^\circ$. So we can also adjust the interaction strength through the angle θ .

3. Experimental setup

In our experiment, the trapping beam (ALS-IR-1064, Azur Light Systems, $\lambda = 1064\text{nm}$) is expanded threefold to overfill the aperture requirements of the SLM (PLUTO-2-NIR-149, HOLOEYE) and the microscope objective (MO, TU Plan ELWD, Nikon, $100\times$, $\text{NA} = 0.8$). The reflected beam from the SLM passes through a 4f configuration composed of lenses L1 and L2, both with focal lengths of 300 mm. This 4f configuration restores the phase profile generated by the SLM to the front focal plane of the MO. The total power of the beam in front of the vacuum

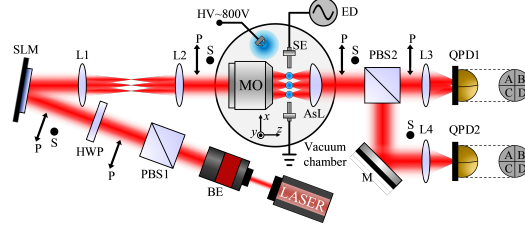


Fig. 3. Schematic of the experimental setup. A 1064 nm trapping beam passes through a beam expander (BE, BE03-1064, Thorlabs) and is incident on a spatial light modulator (SLM), using phase modulation to generate three optical traps. A high-voltage DC power supply (HV \sim 800V) is connected to a pair of bare wires inside the vacuum chamber to change the net charge of the particles through corona discharge. Furthermore, an electric driving signal (ED) is fed into a pair of steel electrodes (SE) to monitor the number of charges by driving the particles. The particles' signals are synchronously recorded by quadrant photodetectors QPD1 and QPD2. PBS, polarizing beam splitter; HWP, half-wave plate; L, lens; MO, microscope objective; AsL, aspheric lens; M, mirror.

chamber is approximately 2.5 W. To generate three optical traps with different linear polarization, we encoded a binary phase grating with a deflection phase on the SLM. Since the SLM can only modulate the beam polarized along its long display axis (the p-polarized direction in Fig. 3), the modulated component of the beam forms trap 1 and trap 3 with nearly equal power at the focal plane, while the remaining component of the beam (mainly s-polarized light) forms trap 2. We can adjust the p-polarized and s-polarized components in the beam by rotating the half-wave plate, thereby modulating the power ratio between trap 1 (trap 3) and trap 2. Additionally, we can adjust the positions of the traps and the phase differences between the traps by changing the encoded phase profile on the SLM.

We created a pressure of \sim 2 mbar in the vacuum chamber to maintain the particles in thermal equilibrium with the environment. We employ a high-voltage DC power supply to generate plasma containing positive and negative ions to adjust the net charge of the particles. Meanwhile, a pair of steel electrodes aligned along the x axis applies an electric driving signal near the traps. We demodulate the oscillation amplitude and phase of particles driven by an electric signal, thereby enabling the neutralization of net charge and the elimination of electrostatic interactions between the particles (see Section 2 of Supplement 1). An aspheric lens (AL1512-C, Thorlabs, NA = 0.55) is set up behind the traps to collimate the forward-scattered beam. Then the beam passes through a polarizing beam splitter (PBS2), where the signal of particle 2 is reflected, while the signals of particle 1 and particle 3 remain in the transmitted beam. The signals of different particles are synchronously detected by different quadrant photodetectors. The x -mode signals are used to control the net charge of the particles, and the z -mode signals are converted into power spectral density (PSD) to characterize the interactions between the particles.

4. Phase-dependence of interactions

The interactions between particle 1 and particle 3 mediated by particle 2 depend on the phase difference $\Delta\varphi$. To verify this, we extract the normal mode splitting $|\omega_2 - \omega_1|$ from the PSD of the z -mode signals at a fixed distance $d = 3.01 \mu\text{m}$, angle $\theta = 45^\circ$ and power difference $\eta \approx -0.24$. In this case, $k_2 \approx 0$, indicating that there are almost conservative interactions, and $k_1 \propto \cos(\Delta\varphi)$. Since trap 1 and trap 3 are modulated by the phase profile on the SLM, we can simultaneously change their phases by adding an overall additional phase to the phase profile. And trap 2 is not generated by the SLM, so its phase remains unchanged. Therefore, we can

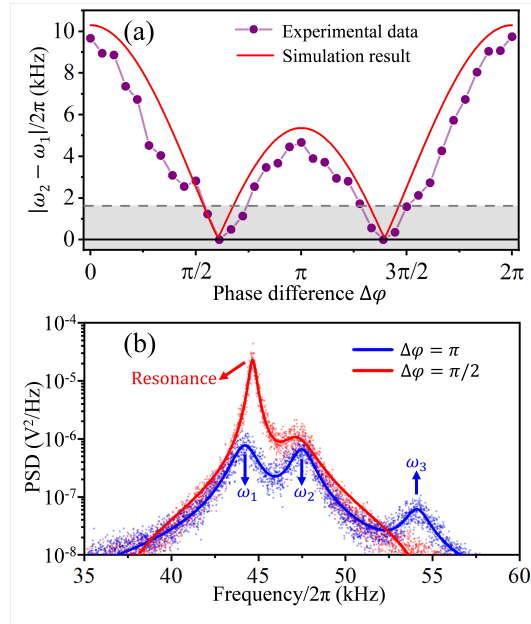


Fig. 4. (a) The normal mode splitting, defined as $|\omega_2 - \omega_1|$, varies with the phase $\Delta\phi$ when $d = 3.01 \mu\text{m}$, $\theta = 45^\circ$, and $\eta \approx -0.24$. The purple dots represent the experimentally measured normal mode splitting. The red curve represents the simulation results incorporating the intrinsic mechanical frequencies Ω_1 , Ω_2 , and Ω_3 under experimental conditions. When the normal mode splitting is smaller than the mechanical linewidth γ (indicated by the dashed gray line), the avoided crossing is indiscernible. (b) The PSD of the z -mode signal is shown for cases where conservative interactions dominate (blue data, $\Delta\phi = \pi$) and where non-conservative interactions dominate (red data, $\Delta\phi = \pi/2$) when $d = 2.80 \mu\text{m}$, $\theta = 45^\circ$, and $\eta \approx -0.05$.

change the phase difference $\Delta\phi$ between trap 1 and trap 2, as well as the phase difference $\pi - \Delta\phi$ between trap 2 and trap 3, while keeping the phase difference between trap 1 and trap 3 fixed at π . In the experiment, we scanned the phase difference from $\Delta\phi = 0$ to $\Delta\phi = 2\pi$ and obtained the changes in normal mode splitting $|\omega_2 - \omega_1|$, as indicated by the purple dots in Fig. 4(a). It is worth noting that the intrinsic mechanical frequencies Ω_1 and Ω_3 of particle 1 and particle 3 are not exactly the same under the current experimental parameters. This discrepancy leads to a deviation between our experimental results and the theoretical model mentioned in the previous section. To mitigate this effect, we recorded the values of Ω_1 , Ω_2 and Ω_3 when the interactions between particles were turned off. We incorporated these values into the theoretical model to obtain the simulation results of the normal mode splitting $|\omega_2 - \omega_1|$ at different phase differences $\Delta\phi$, as shown by the red curve in Fig. 4(a). In the figure, $|\omega_2 - \omega_1|$ closely follows the simulation results, though it is slightly smaller. At $\Delta\phi = n\pi$ (where $n \in \mathbb{Z}$), the normal mode splitting reaches its maximum value, as does the conservative part of the interactions. When the phase difference reaches $\Delta\phi \approx 0.61\pi$ or $\Delta\phi \approx 1.39\pi$, the normal mode splitting approaches zero, indicating minimal conservative interactions. Furthermore, if Ω_1 and Ω_3 are equal, the normal mode splitting $|\omega_2 - \omega_1|$ varies approximately proportionally to $|\cos(\Delta\phi)|$, consistent with the variation of $|k_1|$ with $\Delta\phi$.

In order to further illustrate the effect of non-conservative interactions on the normal modes of the three-particle system, we recorded the PSD of particle 1 and particle 3 at $d = 2.80 \mu\text{m}$, $\theta = 45^\circ$, and $\eta \approx -0.05$ (where both conservative and non-conservative interactions are present),

as shown in Fig. 4(b). When the phase difference reaches $\Delta\varphi = \pi$, the conservative interactions dominate, resulting in non-degenerate normal modes with typical mode splitting. However, when the phase difference reaches $\Delta\varphi = \pi/2$, the non-conservative interactions dominate, causing two of the normal modes to become degenerate. It results in resonance and a significant amplification in the amplitude of particle motion. In our experiment, the presence of non-conservative interactions makes it difficult to observe normal mode splitting and may even lead to particle escape.

5. Position-dependence of interactions

The propagation of the dipole scattering field is influenced by the distance, so the relative positions of the particles modulate the strength of the dipole-dipole interactions. Specifically, as the interparticle distance d changes, the coupling coefficient not only decreases with d^{-1} but also exhibits periodic oscillations due to the decay and phase changes of dipole scattering in the far field. In our three-particle system, when the angle is $\theta = 45^\circ$, the oscillation period will be $\sqrt{2}\lambda$. Since the non-conservative interactions are not well reflected in the normal mode splitting, we set $\Delta\varphi = 0$ to make the conservative interactions dominant. In this case, $k_1 \propto \cos(\sqrt{2}kd/2)/kd$. Similarly, the normal mode splitting $|\omega_2 - \omega_1|$ should exhibit oscillations with a period of $\sqrt{2}\lambda/2$ and decay with d^{-1} . In our experiments, imperfections in the optical path cause slight variations in the power of the trapping beams through the MO as the interparticle distance changes. This results in certain variations in the intrinsic mechanical frequencies of the particles. Therefore, we recorded the intrinsic mechanical frequencies Ω_1 , Ω_2 , and Ω_3 at each distance d without interactions and incorporated them into the theoretical model to obtain the simulation results for the normal mode splitting at different distances. As shown in Fig. 5(a), the curve of experimental data closely matches the curve of simulation results curve, but is slightly smaller. The normal mode splitting displays oscillations with a period of $\sim \sqrt{2}\lambda/2$ and an atypical decay. If Ω_1 and Ω_3 are equal, the decay of the normal mode splitting $|\omega_2 - \omega_1|$ will be closer to the theoretical prediction.

Additionally, we presented the PSD of particle 1 and particle 3 at interparticle distances $d = 3.01 \mu\text{m}$, $3.43 \mu\text{m}$, $3.81 \mu\text{m}$, and $4.24 \mu\text{m}$, as shown in Fig. 5(b-e). It can be observed that at different distances, the normal modes vary between maximum splitting and no splitting. This demonstrates that controlling the interparticle distance d allows us to precisely adjust the strength of the conservative interactions between particle 1 and particle 3. Moreover, by further adjusting $\Delta\varphi$, it is also possible to achieve control over the non-conservative interactions.

In addition to adjusting the interaction strength between particles 1 and 3 by changing the interparticle distance, we can also adjust it by varying the angle θ , which only requires changing the position of particle 2. We set the distance between particle 1 and particle 3 at $3.01 \mu\text{m}$, with $\eta \approx -0.05$ and $\Delta\varphi = 0$, and varied the angle θ from 35.4° to 60.9° . Fig. 5(f) shows the curves of experimental data and simulation results of the normal mode splitting $|\omega_2 - \omega_1|$. The intrinsic mechanical frequencies Ω_1 and Ω_3 are nearly identical under these experimental conditions. The normal mode splitting observed in the experiment reaches its maximum around $\theta = 45^\circ$, which is close to the maximum value predicted by the simulation results. The curve of experimental data almost matches the simulation results for $\theta < 50^\circ$. However, for $\theta > 50^\circ$, the change in normal mode splitting lags behind the simulation results. This may be due to several factors, such as deviations in the interparticle distances caused by radiation pressure from dipole radiation, or deviations in the polarization of trap 2 (the diffraction efficiency of the SLM is about 93%, resulting in a portion of unmodulated light in trap 2, so its polarization is not completely linear). Nonetheless, we can still demonstrate that it is possible to adjust the strength of the conservative interactions between particle 1 and particle 3 by controlling the angle θ . Notably, this adjustment can be achieved by changing the position of particle 2 without moving particles 1 and 3, which highlights the advantage of applying our configuration to optical trap arrays.

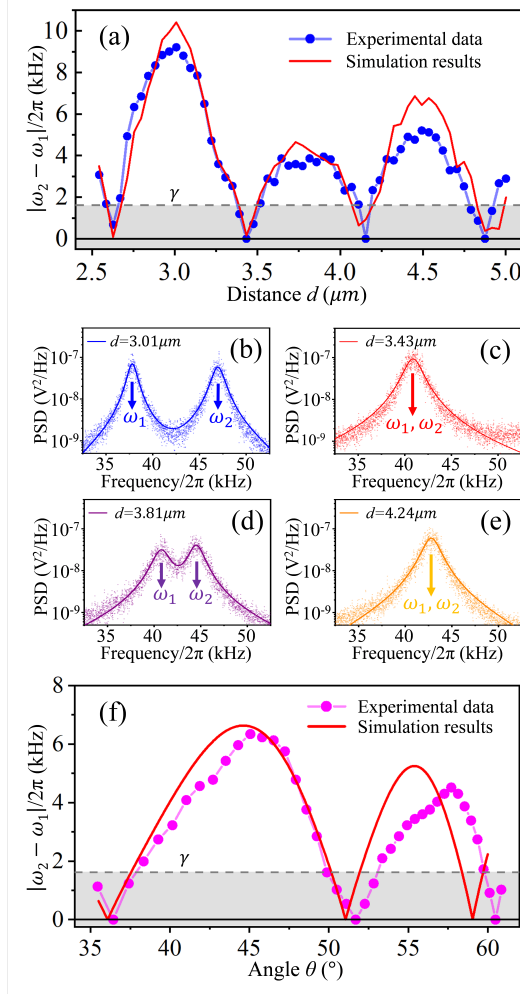


Fig. 5. (a) The normal mode splitting $|\omega_2 - \omega_1|$ as a function of interparticle distance d is shown for $\theta = 45^\circ$, $\eta \approx -0.24$, and $\Delta\varphi = 0$. The blue dots represent the experimentally measured normal mode splitting, while the red curve depicts the simulation results incorporating the intrinsic mechanical frequencies Ω_1 , Ω_2 , and Ω_3 for varying distances. The curve exhibits a periodicity of $\sim \sqrt{2}\lambda/2$. The avoided crossing is unresolved when the splitting is smaller than the mechanical linewidth γ (indicated by the dashed gray line). (b-e) The PSD of the z -mode signals is presented for interparticle distances $d = 3.01 \mu\text{m}$, $3.43 \mu\text{m}$, $3.81 \mu\text{m}$, and $4.24 \mu\text{m}$ with $\theta = 45^\circ$, $\eta \approx -0.24$, and $\Delta\varphi = 0$. At these distances, the normal modes ω_1 and ω_2 exhibit variations between maximum splitting and no splitting. (f) The normal mode splitting $|\omega_2 - \omega_1|$ as a function of the angle θ is shown for $d = 3.01 \mu\text{m}$, $\eta \approx -0.05$, and $\Delta\varphi = 0$. The magenta dots represent the experimentally measured normal mode splitting, while the red curve illustrates the simulation results. As the angle θ varies from 35.4° to 60.9° , $|\omega_2 - \omega_1|$ oscillates, with both the period and amplitude of the oscillation gradually decreasing. The gray dashed line represents the mechanical linewidth γ .

6. Conclusion

In summary, we extended the light-induced dipole-dipole interactions between two particles to a system of three particles. By introducing a third particle as a coupler to the existing two particles without interaction, we enabled dipole-dipole interactions mediated by the third particle. This modulation does not require altering the states of the mediated particles, making it applicable to optical trap arrays with fixed positions and polarization, thus expanding the toolbox for complex interacting systems. We also investigated how the interaction strength varies with phase difference and relative positions, demonstrating significant tunability. Our work provides a novel approach for precisely controlling interactions between adjacent particles in complex multi-body systems. This will promote the development of larger-scale, fully programmable arrays of interacting nanoparticles, which are expected to be used in research areas such as enhanced quantum sensing [39], macroscopic quantum mechanics [13–15], and stochastic thermodynamics [38].

References

1. A. Ashkin and J. Dziedzic, “Optical levitation by radiation pressure,” *Appl. Phys. Lett.* **19**, 283–285 (1971).
2. A. Ashkin and J. Dziedzic, “Optical levitation in high vacuum,” *Appl. Phys. Lett.* **28**, 333–335 (1976).
3. A. Ashkin, J. M. Dziedzic, J. E. Bjorkholm, and S. Chu, “Observation of a single-beam gradient force optical trap for dielectric particles,” *Opt. Lett.* **11**, 288–290 (1986).
4. D. L. Butts, “Development of a light force accelerometer,” Ph.D. thesis, Massachusetts Institute of Technology (2008).
5. F. Monteiro, S. Ghosh, A. G. Fine, and D. C. Moore, “Optical levitation of 10-ng spheres with nano-g acceleration sensitivity,” *Phys. Rev. A* **96**, 063841 (2017).
6. D. C. Moore, A. D. Rider, and G. Gratta, “Search for millicharged particles using optically levitated microspheres,” *Phys. review letters* **113**, 251801 (2014).
7. G. Ranjit, M. Cunningham, K. Casey, and A. A. Geraci, “Zeptonewton force sensing with nanospheres in an optical lattice,” *Phys. Rev. A* **93**, 053801 (2016).
8. T. M. Hoang, Y. Ma, J. Ahn, *et al.*, “Torsional optomechanics of a levitated nonspherical nanoparticle,” *Phys. review letters* **117**, 123604 (2016).
9. S. Zhu, Z. Fu, X. Gao, *et al.*, “Nanoscale electric field sensing using a levitated nano-resonator with net charge,” *Photonics Res.* **11**, 279–289 (2023).
10. E. Tang, J. Agudo-Canalejo, and R. Golestanian, “Topology protects chiral edge currents in stochastic systems,” *Phys. Rev. X* **11**, 031015 (2021).
11. A. Militaru, M. Innerbichler, M. Frimmer, *et al.*, “Escape dynamics of active particles in multistable potentials,” *Nat. Commun.* **12**, 2446 (2021).
12. B. Mahault, E. Tang, and R. Golestanian, “A topological fluctuation theorem,” *Nat. Commun.* **13**, 3036 (2022).
13. Z.-Q. Yin, A. A. Geraci, and T. Li, “Optomechanics of levitated dielectric particles,” *Int. J. Mod. Phys. B* **27**, 1330018 (2013).
14. A. K. Chauhan, O. Černotík, and R. Filip, “Stationary gaussian entanglement between levitated nanoparticles,” *New J. Phys.* **22**, 123021 (2020).
15. M. Arndt and K. Hornberger, “Testing the limits of quantum mechanical superpositions,” *Nat. Phys.* **10**, 271–277 (2014).
16. H. Rudolph, U. Delić, M. Aspelmeyer, *et al.*, “Force-gradient sensing and entanglement via feedback cooling of interacting nanoparticles,” *Phys. review letters* **129**, 193602 (2022).
17. P. Barker and M. Shneider, “Cavity cooling of an optically trapped nanoparticle,” *Phys. Rev. A* **81**, 023826 (2010).
18. O. Romero-Isart, M. L. Juan, R. Quidant, and J. I. Cirac, “Toward quantum superposition of living organisms,” *New J. Phys.* **12**, 033015 (2010).
19. D. E. Chang, C. Regal, S. Papp, *et al.*, “Cavity opto-mechanics using an optically levitated nanosphere,” *Proc. National Acad. Sci.* **107**, 1005–1010 (2010).
20. U. Delić, M. Reisenbauer, K. Dare, *et al.*, “Cooling of a levitated nanoparticle to the motional quantum ground state,” *Science* **367**, 892–895 (2020).
21. J. Piotrowski, D. Windey, J. Vijayan, *et al.*, “Simultaneous ground-state cooling of two mechanical modes of a levitated nanoparticle,” *Nat. Phys.* **19**, 1009–1013 (2023).
22. A. Ashkin and J. Dziedzic, “Feedback stabilization of optically levitated particles,” *Appl. Phys. Lett.* **30**, 202–204 (1977).
23. F. Tebbenjohanns, M. L. Mattana, M. Rossi, *et al.*, “Quantum control of a nanoparticle optically levitated in cryogenic free space,” *Nature* **595**, 378–382 (2021).
24. M. Kamba, R. Shimizu, and K. Aikawa, “Optical cold damping of neutral nanoparticles near the ground state in an optical lattice,” *Opt. Express* **30**, 26716–26727 (2022).

25. C. Gonzalez-Ballester, M. Aspelmeyer, L. Novotny, *et al.*, “Levitodynamics: Levitation and control of microscopic objects in vacuum,” *Science* **374**, eabg3027 (2021).
26. V. Peano, C. Brendel, M. Schmidt, and F. Marquardt, “Topological phases of sound and light,” *Phys. Rev. X* **5**, 031011 (2015).
27. N. Goldman, J. C. Budich, and P. Zoller, “Topological quantum matter with ultracold gases in optical lattices,” *Nat. Phys.* **12**, 639–645 (2016).
28. M. Reisenbauer, H. Rudolph, L. Egyed, *et al.*, “Non-hermitian dynamics and non-reciprocity of optically coupled nanoparticles,” *Nat. Phys.* pp. 1–7 (2024).
29. V. Liška, T. Zemánková, P. Ják, *et al.*, “Pt-like phase transition and limit cycle oscillations in non-reciprocally coupled optomechanical oscillators levitated in vacuum,” *Nat. Phys.* pp. 1–7 (2024).
30. H. Hodaie, A. U. Hassan, S. Wittek, *et al.*, “Enhanced sensitivity at higher-order exceptional points,” *Nature* **548**, 187–191 (2017).
31. M. Fruchart, R. Hanai, P. B. Littlewood, and V. Vitelli, “Non-reciprocal phase transitions,” *Nature* **592**, 363–369 (2021).
32. S. A. Loos and S. H. Klapp, “Irreversibility, heat and information flows induced by non-reciprocal interactions,” *New J. Phys.* **22**, 123051 (2020).
33. S. Liu, Z.-q. Yin, and T. Li, “Prethermalization and nonreciprocal phonon transport in a levitated optomechanical array,” *Adv. Quantum Technol.* **3**, 1900099 (2020).
34. H. Xu, U. Delić, G. Wang, *et al.*, “Exponentially enhanced non-hermitian cooling,” *Phys. Rev. Lett.* **132**, 110402 (2024).
35. J. Vijayan, J. Piotrowski, C. Gonzalez-Ballester, *et al.*, “Cavity-mediated long-range interactions in levitated optomechanics,” *Nat. Phys.* pp. 1–6 (2024).
36. J. Rieser, M. A. Ciampini, H. Rudolph, *et al.*, “Tunable light-induced dipole-dipole interaction between optically levitated nanoparticles,” *Science* **377**, 987–990 (2022).
37. F. Yan, P. Krantz, Y. Sung, *et al.*, “Tunable coupling scheme for implementing high-fidelity two-qubit gates,” *Phys. Rev. Appl.* **10**, 054062 (2018).
38. J. Gieseler and J. Millen, “Levitated nanoparticles for microscopic thermodynamics—a review,” *Entropy* **20**, 326 (2018).
39. A. McDonald and A. A. Clerk, “Exponentially-enhanced quantum sensing with non-hermitian lattice dynamics,” *Nat. communications* **11**, 5382 (2020).